Journal of Physics: Condensed Matter

Detailed study of the $CePd_{2-x}Ni_xAl_3$ magnetic phase diagram around its critical concentration

To cite this article: J G Sereni *et al* 2006 *J. Phys.: Condens. Matter* **18** 3789

INSTITUTE OF PHYSICS PUBLISHING JOURNAL OF PHYSICS: CONDENSED MATTER

J. Phys.: Condens. Matter **18** (2006) 3789–3802 doi:10.1088/0953-8984/18/15/022

Detailed study of the $CePd_{2-x}Ni_xAl_3$ magnetic phase diagram around its critical concentration

J G Sereni[1], P Pedrazzini[2], E Bauer[3], A Galatanu[4], Y Aoki[5] and H Sato[5]

[1] Lab. Bajas Temperaturas, Centro Atómico Bariloche (CNEA) and CONICET, RA-8400 S.C. de Bariloche, Argentina
[2] DPMC-Universitè de Genève, Q. E.-Ansermet, CH-1211 Genève, Switzerland
[3] Institut für Festkörperphysik, Technische Universität Wien, A-1040 Wien, Austria
[4] National Institute for Material Physics, Atomistilor 105 bis, Bucharest-Magurele, POB MG-07, 077125, Romania
[5] Department of Physics, Tokyo Metropolitan University, Minami-Ohsawa 1-1, Hachioji-Shi, Tokyo 192-0397, Japan

E-mail: jsereni@cab.cnea.gov.ar

Received 14 December 2005, in final form 5 March 2006
Published 30 March 2006
Online at stacks.iop.org/JPhysCM/18/3789

Abstract

Thermal, magnetic and transport measurements on $CePd_{2-x}Ni_xAl_3$ alloys within the $0 \leqslant x \leqslant 1$ range are reported, including applied pressure (p) and magnetic field on some selected samples. The low temperature results indicate that long range antiferromagnetic order is robust up to $x = 0.2$, whereas between 0.25 and 0.5 magnetic fluctuations give rise to non-Fermi-liquid (NFL) behaviour. In this critical region, the low temperature specific heat can be described as due to two components, the major showing a NFL $C_p/T = \gamma_0 - \gamma_1\sqrt{T}$ dependence, while the minor one includes a decreasing fraction of short range order degrees of freedom. The latter is only observed close to the critical point, $x_{cr} \approx 0.35$. Electrical resistivity (ρ) studies performed under pressure for $x = 0.5$ allow us to investigate the evolution of the NFL state around and beyond x_{cr}, where the exponent of $\rho \propto T^n$ increases from $n = 1$ (for $p = 0$) up to $n = 2$ (for $p = 12$ kbar). This exponent is also observed at normal pressure on the $x = 1.0$ sample, indicating the onset of the Fermi liquid behaviour. Doping and pressure effects are compared by fitting high temperature resistivity data employing a unique function which allows us to describe the evolution of the characteristic energy of this series along a large range of concentration and pressure.

1. Introduction

Numerous magnetic phase diagrams of Ce-lattice systems have been investigated in recent years motivated by novel physical properties observed around their magnetic instability region.

In these systems the variation of the ordering temperature (T_N) is currently driven by controlling parameters like pressure (p), Ce-ligand substitution (x) or magnetic field (H). The low temperature divergences observed in their thermodynamic parameters correspond to a non-Fermi-liquid (NFL) behaviour [1–3], indicating the vicinity of a quantum critical point (QCP) at $T = 0$. This is a consequence of substantial modifications in the nature of the fluctuations related to the magnetic transition. The possibility of experimental access to this new regime, where quantum fluctuations compete in energy with the thermal ones, has concentrated a significant effort on the study of novel magnetic phase transitions.

Because a QCP occurs at zero temperature, it is frequently found that some magnetic phase diagrams include naïve extrapolations for $T_N(x, p) \to 0$. A strict analysis of the experimental results indicates that only in a few Ce-lattice systems can $T_N(x, p)$ be unambiguously traced down to very low temperature, i.e. at least down to $T_N(x, p)/T_N(0, 0) < 0.1$ [4] as in $CeCu_{6-x}Au_x$ [5] or $CeIn_{3-x}Sn_x$ [6].

In the scope of Doniach's model [7], the description of a magnetic phase diagram is governed by two relevant parameters: T_N and T_K, which depend on the same coupling parameter (J_{ex}) between local moments and conduction electron spins. Nevertheless, different doping and pressure dependences were experimentally observed for T_N and T_K in Ce-lattice systems [8]. There are, for example, systems where $T_N(x, p)$ decreases while T_K practically does not change, while others show a weak doping or pressure dependence of T_N, while T_K increases monotonically. It is therefore of great interest to perform detailed experimental investigations on such Ce systems to unambiguously determine the $T_K(x, p)$ behaviour throughout the transition between their magnetic and non-magnetic phases.

From previous studies on its physical properties, $CePd_{2-x}Ni_xAl_3$ [9, 10] can be considered as an exemplary candidate for such a purpose. By doping Pd sites with smaller (but electronically equivalent) Ni atoms it is possible to induce a continuous change from antiferromagnetic $CePd_2Al_3$ ($T_N = 2.8$ K [9]) to non-magnetic $CeNi_2Al_3$ [11]. In this system $T_N(x, p)$ and the related specific heat jump (ΔC_m) are weakly affected by Ni doping up to $x = 0.2$ [12–14] and pressure [15]. Above that concentration, ΔC_m transforms into a broad anomaly [14]. An advantage of this system is that doping effects can be compared with pressure studies performed on stoichiometric $CePd_2Al_3$ [10, 16], where T_N vanishes at $\approx$12 kbar. Keeping in mind these features, we have performed a more detailed and comprehensive investigation on thermal, magnetic and transport properties of this system, including for such a purpose new samples with Ni content tuned on the critical concentration. The present investigation also includes electrical resistivity measurements under pressure and magnetic field on some selected concentrations. This procedure allows a unique quantitative comparison between three experimental control parameters: alloying, pressure and magnetic field. Altogether, this wide amount of information permits us to access a unified description of this system covering its complex behaviour around its critical concentration and to compute the evolution of its characteristic energy scale over more than one decade.

2. Experimental details

Samples with Ni concentrations in the range $0.03 < x < 1$ were prepared by melting appropriate amounts of elements using a high frequency melting procedure and subsequent heat treatment at $T = 900\,^{\circ}$C for two weeks [12]. No foreign phases were detected from x-ray diffraction patterns obtained applying Co Kα radiation. Specific heat measurements on samples of about 1 g were performed in a semi-adiabatic calorimeter at temperatures ranging from 0.2 up to 30 K, using a heat pulse technique. A standard SQUID magnetometer served for the determination of the magnetization from 2 K up to room temperature in a 1 T magnetic

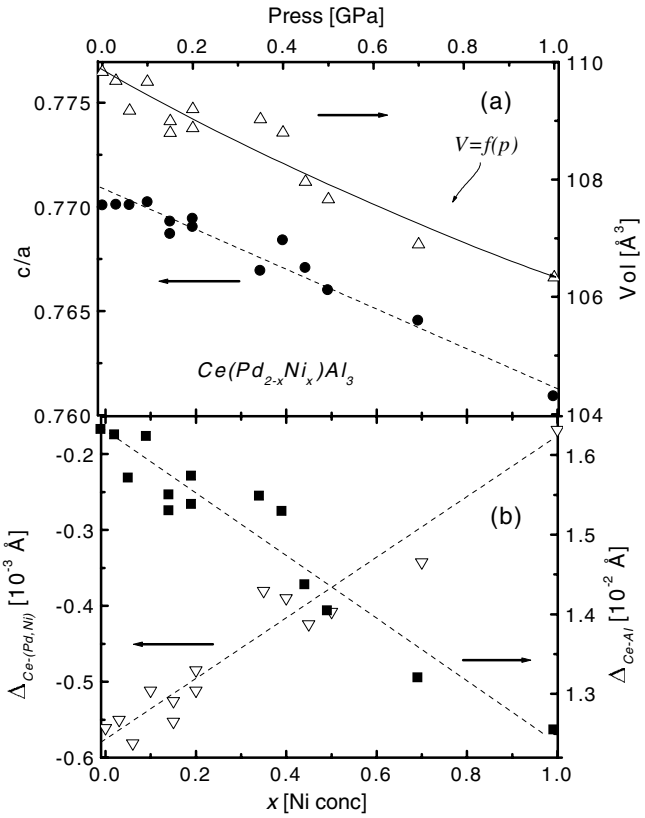

Figure 1. (a) Lattice parameter ratio c/a (left side) and unit cell volume V (right side) as a function of Ni concentration. The solid line indicates the volume (right side) dependence on pressure (top axis) of $CePd_2Al_3$, after [10]. (b) Comparison of the effective interatomic spacings with respect to those of pure elements (see the text).

field. The ac susceptibility of one of the samples was measured down to 0.5 K using the mutual inductance technique with a lock-in amplifier as detector working at 12.8 kHz with an excitation amplitude of $\approx 10\ \mu$T. The electrical resistivity and magnetoresistivity were measured using a four probe dc method in the temperature range from 0.5 K up to room temperature and fields up to 12 T. A piston–cylinder pressure cell with a paraffin mixture as pressure transmitter served to generate hydrostatic pressure up to about 12 kbar. The absolute value of the pressure was determined from the superconducting transition temperature of lead.

3. Results

3.1. Lattice parameters

The evolution of structural parameters with increasing Ni concentration is shown in figure 1. As expected from the relative atomic volumes of the pure elements (Ni and Pd), the molar volume (V_m) of $CePd_{2-x}Ni_xAl_3$ decreases with increasing Ni content at a rate $(\Delta V/V_m)/\Delta x = d\ln V/dx = 0.033(2)$/Ni at. (see figure 1(a)). The 'c/a' ratio between the lattice parameters of this hexagonal system decreases by about 1.3% per Ni atom, producing a slight modification in the relative positions of the Ce-neighbouring atoms. For a more detailed analysis, we have evaluated the corresponding interatomic distances as $d_{Ce-TM} = a\sqrt{3}$ and $d_{Ce-Al} =$

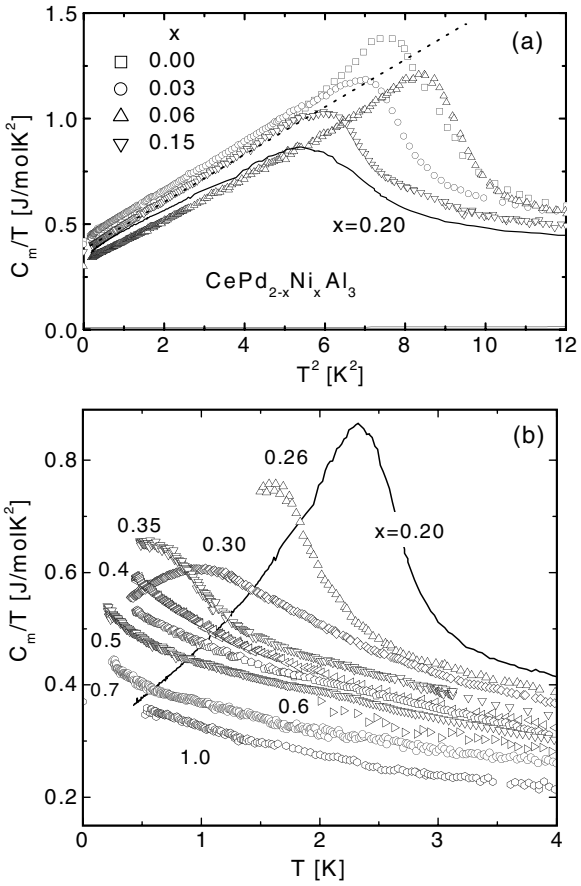

Figure 2. Magnetic contribution to the specific heat C_m divided by T. (a) In a C_m/T versus T^2 representation for the samples with $x \leqslant 0.20$. The dotted line represents a $\gamma + BT^2$ function (see the text). (b) Linear temperature dependence for the $x \geqslant 0.2$ samples to show the C_m/T versus T evolution around the critical concentration. Results for $x = 0.26$ and 0.6 are taken from [14].

$1/2\sqrt{a^2 + c^2}$, where TM indicates Pd or Ni. These distances are compared in figure 1(b) with the respective atomic radius ($r_{Ce^{3+}} = 1.86$ Å, $r_{Pd} = 1.37$ Å, $r_{Ni} = 1.25$ Å and $r_{Al} = 1.43$ Å [17]), computing an effective interatomic spacing as $\Delta_{Ce-Z} = d_{Ce-Z} - (r_{Ce^{3+}} + r_Z)$ (with Z = TM or Al). In a simple rigid-sphere picture, $\Delta_{Ce-Z} < 0$ indicates a reduction of the Ce Wigner–Seitz cell with respect to that of pure metal. Despite the reduction of $V_m(x)$, the positive slope of $\Delta_{Ce-TM}(x)$ indicates that the Ce–TM overlap becomes weaker with Ni doping. In contrast, Δ_{Ce-Al} decreases with doping. From this comparison we conclude that the volume decreases as a whole upon increasing Ni content; the main mechanism of enhancing 4f-orbital hybridization is, however, a shortening of the Ce–Al distance.

3.2. Specific heat

The magnetic contribution to the specific heat (C_m) is obtained by subtracting the phonon contribution (C_{ph}) from the measured values: $C_m = C_P - C_{ph}$, where $C_{ph} = 0.3 \times 10^{-3}$ J mol^{-1} K^{-2} $\times T^3$ was extracted from the reference compound $LaPd_2Al_3$. Data for the samples with $x \leqslant 0.20$ are displayed in figure 2(a) using a C_m/T versus T^2 representation

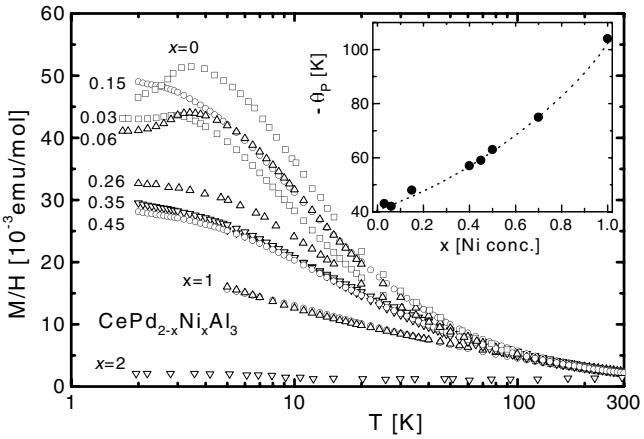

Figure 3. Temperature dependent magnetization divided by applied field (1 T), in a semi-logarithmic representation. Results for $x = 0.26$ [14], 1.0 [12] and 2.0 [11] are included for comparison. Inset: θ_P increase as a function of Ni concentration.

to better show the canonical antiferromagnetic dispersion relation. The observed $C_m/T = \gamma + BT^2$ dependence for $T < T_N$ corresponds to long range antiferromagnetic (AF) order, where $B \propto J_{ex}^{-3}$ [18]. Because the parameter B is almost independent of concentration ($B = 0.11 \pm 0.01$ J mol^{-1} K^{-4}), one concludes that J_{ex} has no significant variation up to $x = 0.20$. Beyond $x = 0.20$ a clear change of $C_m(T)/T$ is observed at $T \leqslant T_N$ (see figure 2(b)). The C_m/T peak at T_N transforms into a broad anomaly, which decreases up to $x = 0.30$. Coincidentally, the temperatures of these maxima extrapolate to zero at $x \approx 0.40$. At higher Ni concentration no magnetic transition is observed down to 0.4 K.

3.3. Magnetic susceptibility

The temperature dependence of the magnetic susceptibility for samples with $x \leqslant 0.45$ is shown in figure 3 in a semi-logarithmic representation. These results are compared with those reported in the literature for $x = 0.26$ [14], $x = 1$ [12] and $x = 2$ [11]. While at high temperature nearly the full magnetic moment ($\mu_{eff} = 2.54\ \mu_B$) of the Ce ion is observed, the deviation from the Curie–Weiss law at low temperature indicates a weakening of the effective moment owing to the reduction of the thermal population of excited crystal field (CEF) levels. In these measurements, a well defined maximum at T_N is evident for samples exhibiting long range magnetic order (LRMO). In contrast, for samples with $x > 0.2$ there is a tendency to saturation at low temperature with a magnetization (evaluated at $T = 2$ K) dropping from 0.05 to 0.028 emu mol^{-1} between $x = 0.15$ and 0.45.

In the inset of figure 3 we show the concentration dependence of the Curie–Weiss temperature $\theta_P(x)$, extrapolated from $T > 200$ K. As expected, the negative values of θ_P increase monotonically with Ni concentration from $\theta_P(x = 0) \approx -40$ K up to ≈ -100 K for $x = 1$. This concentration dependence of θ_P may result from two competing contributions: (i) the antiferromagnetic interaction between Ce moments and (ii) the increasing Kondo temperature. While the former decreases as the Ce magnetic moments weaken, the latter increases with T_K [19]. Therefore, the latter is expected to dominate the value of θ_P once $\theta_P \gg T_N$. Reasonable values of T_K can be derived using the standard single impurity Kondo model with $T_K \approx |\theta_P|/4$ [20].

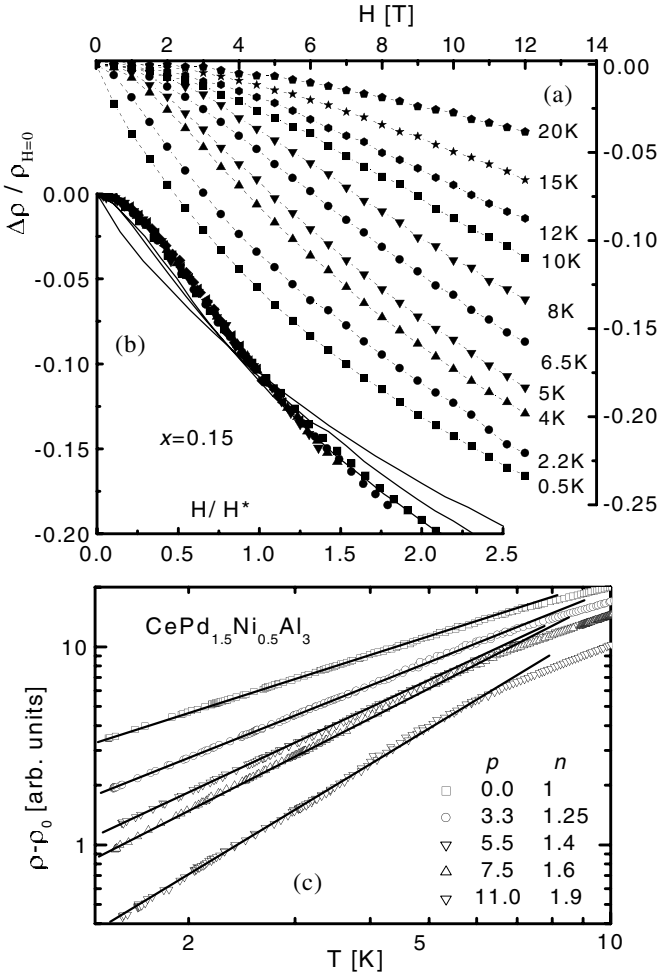

Figure 4. (a) Isothermal magnetoresistance $\Delta\rho/\rho$ of $x = 0.15$ at different temperatures. (b) Magnetoresistance as a function of the normalized magnetic field H/H^* (symbols for $T > T_N$ and lines for $T \leqslant T_N$). (c) Low temperature resistivity of $x = 0.50$ plotted as $\rho(T) - \rho_0$ versus T in a double logarithmic scale, where ρ_0 is the residual resistivity and the slope n is a function of pressure (p (kbar)).

3.4. Electrical resistivity

The thermal dependence of the electrical resistivity (ρ) of these alloys was investigated as a function of Ni concentration, hydrostatic pressure (p) and magnetic field (H), providing valuable information concerning the evolution of the ground state under different control parameters. In order to evaluate the role of the Kondo effect in the AF phase, we have studied $\rho(H, T)$ of sample $x = 0.15$ up to $H = 12$ T. Experimental values obtained from isotherms between 0.5 K $\leqslant T \leqslant$ 20 K are collected in figure 4(a) as $\frac{\Delta\rho}{\rho}$ versus H, where $\frac{\Delta\rho}{\rho} = \frac{\rho(H)-\rho(0)}{\rho(0)}$. Above T_N, the variation of $\Delta\rho/\rho$ is well scaled by a reduced magnetic field (H/H^*) as predicted for Kondo systems [21], where $H^* = (1+1.5T)k_B/\mu_{eff}$ (see figure 4(b)). As expected, deviations from such a scaling are observed for $T < T_N$ (solid curves). Similar scaling (not shown) is obtained for $x = 0.06$.

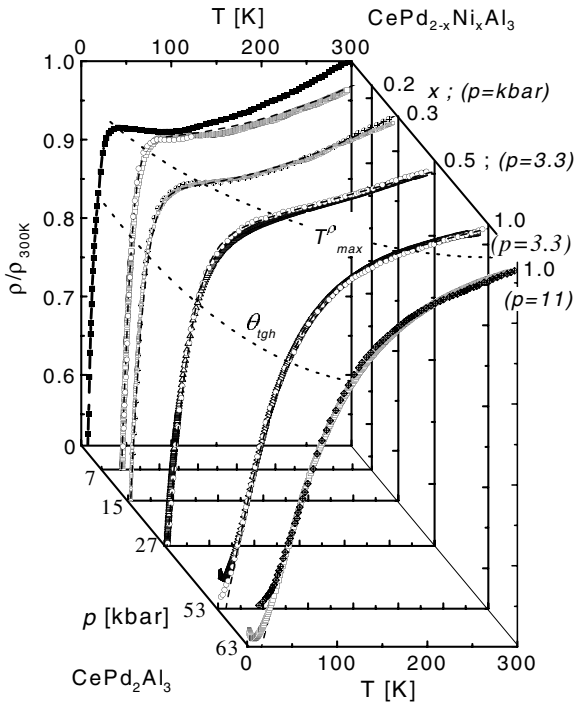

Figure 5. Normalized electrical resistivity of some selected Ni-doped samples: $x = 0.20, 0.30, 0.50$ (at 3.3 kbar) and 1.0 (at 3.3 and 11 kbar) (top right axis), in comparison with the resistivity of stoichiometric $CePd_2Al_3$ [16] at different pressures: $p = 0, 7, 15, 27, 53$ and 63 kbar (bottom left axis). $T^{\rho}_{\max}$ (dotted curve) indicates the concentration dependent evolution of the temperature of the resistivity maximum and θ_{tgh} (dashed curve) is a fitting parameter used for comparison (see the text).

Around the critical concentration, the NFL behaviour is identified by a power law dependence of the electrical resistivity, $\rho(T) \propto T^n$. In order to better establish the actual extension of the NFL region on the non-magnetic side of the critical region, we have analysed the $\rho(T)$ dependence of the $x = 0.20$ and $x = 0.50$ samples up to $p = 12$ kbar [12]. Results for $x = 0.5$ are displayed in figure 4(c), in a double logarithmic representation, with the data normalized to their respective values at room temperature. The exponent $n(x, p)$ is extracted from the slope of a linear fit at low temperature after subtracting the residual resistivity ρ_0. Due to the proximity of the $x = 0.50$ sample to the critical point there is a significant variation of this exponent from $n = 1$ ($p = 0$) up to $n = 1.9$ ($p = 11$ kbar), as expected for a system driven to a Fermi liquid (FL) state by pressure. A similar procedure was applied to the samples $x = 0.20$ and $x = 1$; the former exhibits a pressure driven increase of n and the latter is already placed at the edge of the FL state (i.e. $n = 2$) at normal pressure. Despite the narrow temperature range from which these exponents are extracted, the evolution of $n = n(x, p)$ provides relevant information and will be further discussed in the context of figure 7.

High temperature resistivity measurements were performed on samples ranging between $x = 0.10$ and 1, and under pressures up to 12 kbar. In figure 5 we compare the $\rho(T)/\rho_{300\text{ K}}$ dependence of some selected samples ($x = 0.20; 0.30; 0.50$ [12] and 1.0) with that of the stoichiometric compound $CePd_2Al_3$ [16] at different values of applied pressures ($p = 0$; 7; 15; 27; 53 and 63 kbar). For clarity, only the $\rho(T, p)$ results of $CePd_2Al_3$ coinciding with

those from different Ni alloys (either at ambient conditions or under pressure) are included in the figure. These coincidences are found between $p = 7$ kbar on $CePd_2Al_3$ and $x = 0.20$, $p = 15$ kbar and $x = 0.30$, $p = 27$ kbar and $x = 0.50$ under 3.3 kbar and $p = 53$ (and 63) kbar with $x = 1$ under 3.3 (and 11) kbar respectively. The electrical resistivity of the reference compound $LaPd_2Al_3$ (not included) was also measured to evaluate the phonon contribution at high temperature. There, the slope of $\rho(T)$ at high temperature is very similar to that of Ce compounds. The temperature of the maximum of $\rho(T)$ ($T^{\rho}_{\max}$) is also depicted in figure 5 to show how it increases with Ni doping from about 28 K in $CePd_2Al_3$ up to above room temperature in $CePdNiAl_3$. Already at $x = 0.50$ that maximum becomes so wide that it mixes with the phonon contribution, impeding any precise determination.

4. Discussion

The specific heat jump at T_N determines the magnetic phase boundary as a function of concentration up to $x = 0.20$. As mentioned above, up to that concentration the $C_m(T_N)$ jump is followed at lower temperatures by a $\propto T^3$ dependence which characterizes a stable AF phase [18]. Beyond $x = 0.20$ the maximum of C_m/T broadens and decreases, both in height and temperature. These are indications that the LRMO collapses into short range magnetic interactions. Such a collapse may be related to a geometric frustration, originated in a distortion of the triangular configuration of magnetic atoms as proposed in [9]. However, at $x = 0.30$ the tendency is partially reversed and the maximum C_m/T slightly increases again. Owing to this change of regime occurring in the proximity of the critical point, we have performed a detailed analysis of the $C_m(T)/T$ dependences of the alloys included in the $0.30 < x \leqslant 0.50$ range. As shown in figure 6(a), the measurements are well described by an expression accounting for two contributions: $C_m(T)/T = C_{NFL}/T + C_R/T$, where C_{NFL}/T is described by a non-Fermi-liquid temperature dependence and C_R/T includes a remnant magnetic contribution. The usual T dependences of C_P/T in NFL systems are [2] $-\log(T/T_0)$; $\gamma_0 - \gamma_1\sqrt{T/T_0}$ or a T^{-q} power law. We see that within this concentration range the $\sqrt{T/T_0}$ dependence, proposed in terms of three-dimensional AF spin-fluctuation theories [22], provides the best description for the experimental results. As a consequence of this analysis we infer that the majority fraction of degrees of freedom corresponds to a NFL component (dotted lines in figure 6(a)). On the other hand, the entropy related to C_R/T extrapolates to zero for $x \approx 0.50$ together with the temperature of the maximum of $C_m(T)/T$. Ac-susceptibility measurements performed for $x = 0.35$ (not shown) confirm the anomaly in the specific heat as due to a weak magnetic transition.

Since the phonon contribution is negligible compared to that of the 4f electrons, and also that due to CEF excitations is marginal in this temperature range, at least below ≈9 K, the fitted data correspond to the electronic ground state (GS) contribution only. Hence, the entropy S_m calculated from C_m/T contains the degrees of freedom from both C_{NFL}/T and C_R/T. Actually, most of the S_m contribution corresponds to the former ($\gamma_0 - \gamma_1\sqrt{T/T_0}$), with a minor extra contribution of the latter.

The change of $C_m/T(T)$ dependences above T_N between the alloys belonging to the AF region ($x \leqslant 0.30$) and those from the critical one ($0.35 \leqslant x \leqslant 0.50$) reflects a difference in their respective excitation spectra. While the former is well accounted for by $C_m/T \propto -\ln T$ (hereafter called the *reference function*: C_{Ref}/T), the latter exhibits a $\sqrt{T/T_0}$ dependence. Further implications of this change of regime can be searched out investigating $S_m(T, x)$ within the critical region. Since between $x = 0$ and 0.20 the $S_m(T)$ gain between $T = 0$ and $T \geqslant T_N$ is the same as that computed using C_{Ref}/T (hereafter $S_{Ref}(T)$), one concludes that all degrees of freedom condensed in the AF state come from a uniform paramagnetic phase. In figure 6(b)

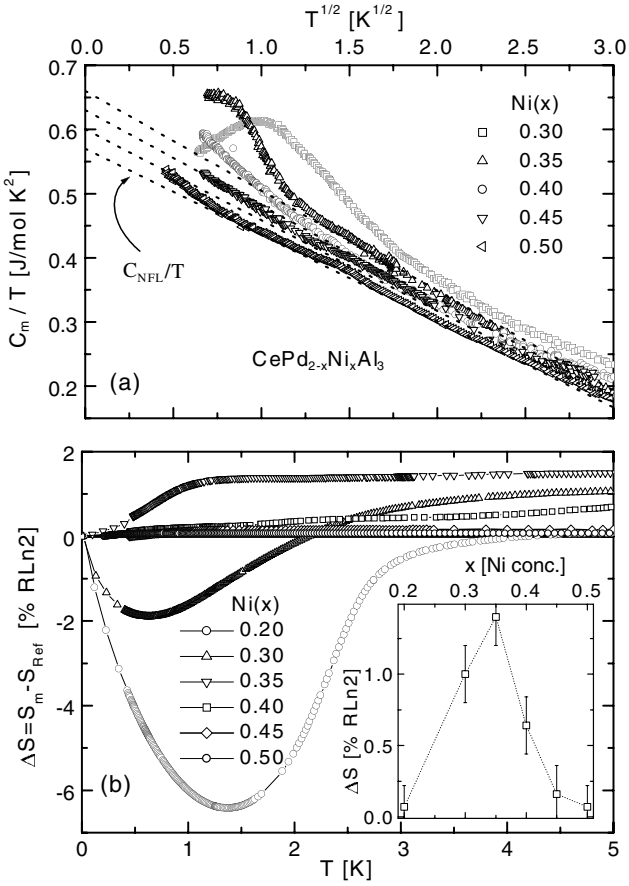

Figure 6. (a) Magnetic contribution to the specific heat plotted as C_m/T versus $\sqrt{(}T)$ for the $0.35 \leqslant x \leqslant 0.45$ samples, to make evident the $C_{NFL}/T = \gamma_0(x)(1 - \sqrt{T/T_0})$ [24] and C_R/T contributions. The $x = 0.30$ sample is included for comparison. Dotted lines are extrapolations to $T = 0$ to extract $\gamma_0(x)$. (b) Entropy difference ΔS between measured and reference values. Inset: ΔS at 5 K, showing its concentration dependence (see the text).

we show how $S_m - S_{Ref}$ vanishes for $x = 0.20$ when $T \geqslant T_N$. However, this analysis performed for $x = 0.30$ already reveals an *additional* contribution to $S_m(T)$, which cannot be accounted for by $S_{Ref}(T)$. Such an extra contribution is better identified in sample $x = 0.35$ because for $x > 0.35$ $C_{Ref}/T = C_{NFL}/T = \gamma_0 - \gamma_1\sqrt{T/T_0}$, that excludes the C_R/T contribution. Since measured $S_m(T < T_N)$ also collects these additional degrees of freedom, $\Delta S = S_m - S_{Ref} > 0$ for $T > T_N$. This difference decreases for $x = 0.40$ and finally vanishes as the system becomes non-magnetic at $x = 0.50$ (see figure 6(b)). This indicates the presence of an *extra* contribution to the internal energy of the system at low temperatures, which only occurs in the vicinity of the critical point. Such a contribution only involves a few per cent of the GS related $R \ln 2$.

Though the origin of this anomaly is unknown, some peculiar characteristics, e.g. the small number of degrees of freedom involved and its location at the critical concentration, hint at the possibility of some instability in the Fermi surface (FS). As the RKKY interaction vanishes, low lying energy excitations related to eventual electronic transitions [23] or any other modification of the FS may become relevant. In this context, a microscopic study of the FS topology is required to verify such an alternative.

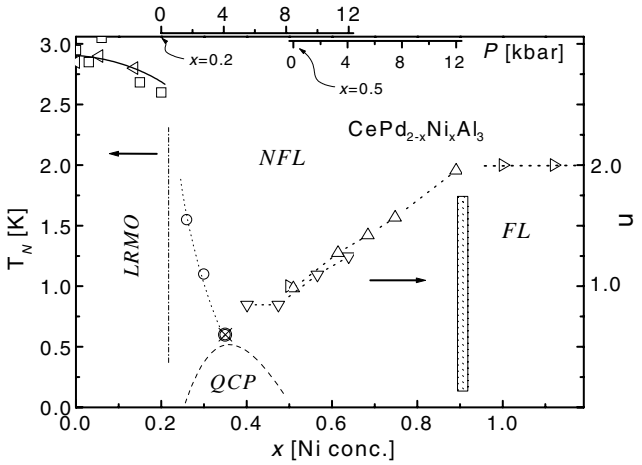

Figure 7. Magnetic phase diagram of $CePd_{2-x}Ni_xAl_3$, with T_N determined from C_m/T, □ and ○, and ac-χ, ⊗, in comparison with the pressure effect on $x = 0$ (◁) [10]. The evolution of the exponent of $\rho \propto T^n$ under pressure (upper axis), applied on samples $x = 0.20$ (▽), 0.50 (△) [12] and 1.0 (▷), was extracted following the procedure shown in figure 4(c). Offsets are taken at the positions of the respective concentrations indicated on the lower axis. The dashed line around the QCP indicates the region where the *extra* entropy is observed.

Beyond the critical concentration, the changes in the magnetic ground state can be traced following the evolution of the exponent n in the $\rho \propto T^n$ dependence, as already quoted for the sample $x = 0.50$ in figure 4(c). Its variation between $1 \leqslant n \leqslant 2$ (for $0 \leqslant p \leqslant 11$ kbar) is an indication that the NFL behaviour dominates the low temperature physical properties even beyond the critical point. The same procedure was applied to $x = 1.0$, where the exponent $n \approx 2$ marks the entrance to the FL. On the other hand, measurements performed on the sample $x = 0.20$ evidence a tuning towards the critical point at $p = 8$ kbar.

We have collected these results in a low temperature phase diagram shown in figure 7, combining Ni concentration with pressure dependences of $\rho(T)$ measured on samples with $x = 0.20, 0.50$ [12] and 1.0. From this analysis one can see that pressure and doping drive the system to the non-magnetic ground state in a similar way, allowing a direct comparison between them. In fact, the properties of $x = 0, 0.20$ and 0.50 samples match each other on the application of pressure. Between the LRMO ($x \leqslant 0.20$) and the FL ($x \geqslant 1.0$) phases there is a region ($0.30 \leqslant x \leqslant 0.40$) where the growing NFL component coexists with an exhausting fraction of remnant magnetic interactions. The critical concentration, around 0.40, is then determined by both $C_m/T = \gamma_0(1-\sqrt{T/T_0})$ and $\rho \propto T^n$. We note that on approaching the critical region (i.e. between $x = 0.30$ and 0.50) T_0 slightly changes between 14 and 17 K whereas $\gamma_0(x)$ decreases linearly from 0.7 to 0.57 J mol^{-1} K^{-2}, according to the increase of T_K.

A general understanding of the phase diagram (see figure 7) follows the implications of Doniach's model [7], in which the ordering of Ce moments due to RKKY interaction and their compensation by the Kondo effect are competing. However, different dependences were experimentally identified when approaching the respective critical points. In an ample comparison of magnetic phase diagrams performed on a large number of Ce systems [4] it was shown that a clear distinction can be made among various types of phase boundaries. These different behaviours can be sorted into three groups recognized through the following characteristics: (i) the already quoted systems with $T_N(x, p) \rightarrow 0$; (ii) those whose phase

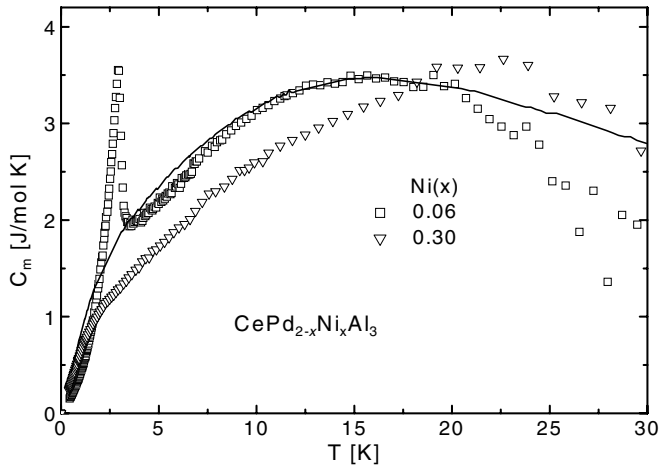

Figure 8. Temperature dependent magnetic specific heat up to 30 K to show the contribution of the first excited CEF doublet. The solid line is a fit according to the model of Desgranges and Rasul [26].

boundaries vanish at finite temperature ($T_N(x, p)/T_N(0, 0) \geqslant 0.4$) and (iii) the systems where T_N is weakly doping or pressure dependent before vanishing. The magnetic phase diagram of the present Ce system can be identified as belonging to group (iii), since its long range magnetic order is weakly doping (pressure) dependent up to $x \approx 0.20$ ($p \approx 10$ kbar).

The first excited CEF level of $CePd_2Al_3$ was found at $\Delta_{CF}^{I} \approx 25$ K from magnetic susceptibility [9] and at 33 K from neutron scattering measurements [25]. From the latter, the Kondo temperature was evaluated as $T_K = 22$ K, that indicates a peculiar characteristic of this system since $T_N \ll T_K$ and $T_K \approx \Delta_{CF}^{I}$. Complementary information can be obtained from our specific heat results, where the contribution of the first excited CEF doublet is observed from measurements up to 30 K as a Schottky anomaly, broadened by the hybridization effect. In figure 8 we show those results for $x = 0.06$ and 0.30. Results derived for $x = 0.06$ are compared with model calculations for a $\Delta_{CF}^{I} = 28$ K splitting and an equal value of T_K [26]. This relatively high value of T_K does not match with the value extracted from $\gamma_0 \propto 1/T_K$ (see figure 6(a)). In order to clarify this aspect we have analysed the entropy gain (ΔS_m) in these samples. Following the definition for a single Kondo impurity model [27], T_K is tentatively defined as the temperature where $\Delta S_m \approx 2/3R \ln 2$. This procedure yields T_K values ranging between 6.3 K for $x = 0.03$ and 15 K for $x = 0.30$. This difference in T_K values derived from measurements below or above 10 K evidence the relevant role of the first excited CEF level in the high temperature range. Hence, one has to distinguish between T_K associated with the GS (T_K^{GS}) and T_K^{CF}, that accounts for the hybridization effects on the excited CEF levels.

In order to analyse the large set of resistivity results obtained as a function of concentration and pressure, we have searched for a parameter allowing us to compare this information. For such a purpose the mentioned maximum $T_{max}^{\rho}(x, p)$ is often used. This maximum, however, is the result of a competition between two different scattering regimes: the incoherent Kondo scattering at high temperature ($T \gg T_{max}^{\rho}$) associated with the first excited CEF level and the coherent one at $T < T_{max}^{\rho}$, which arises from the Ce Kondo lattice behaviour at low temperature. Since the formation of ρ_{max} corresponds to a continuous change of regime, it is intrinsically broad and (as mentioned before) it becomes even wider when it moves to higher temperature (see figure 5), making its evaluation quite speculative above 200 K. To obtain a convenient

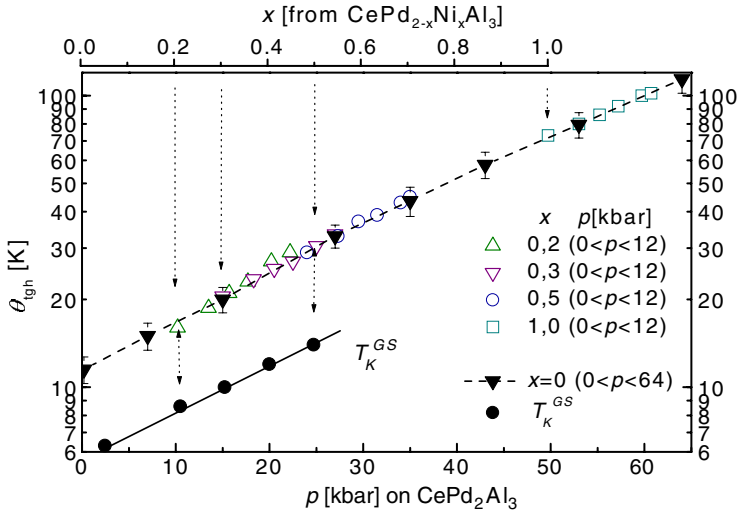

Figure 9. Pressure (lower abscissa) and concentration (upper abscissa) evolution of θ_{tgh} in a semi-logarithmic (ordinate) representation. $p = 0$ origins for different Ni concentrations are located at the respective x values (upper abscissa) and identified by vertical dashed arrows. The dotted curve corresponds to a $d \ln \theta_{tgh}/dx = 2.3$/Ni at. Some $T_K^{GS}(x)$ values are also included (see the text). Representative error bars are shown on the $x = 0$ ($0 < p < 64$ kbar) points.

scaling parameter characterizing the evolution of $\rho(T)$ in a broad range of temperature, a parameter 'θ' can be defined following the Grüneisen criterion:

$$\rho(T) = \rho_0 + \rho_m(T/\theta) + \rho_{ph}(T). \tag{1}$$

For such a purpose we have chosen a heuristic expression for $\rho_m(T/\theta)$ which properly describes the experimental results as

$$\rho(T) = \rho_0 + a \times \tanh(T/\theta_{tgh}) + \rho_{ph}(T) \tag{2}$$

where θ_{tgh} is an *intensive* parameter which scales $\rho_m(T)$ curves and allows us to compare all the resistivity data. $\rho_{ph}(T)$ can be evaluated from the high temperature slope of $\rho(T)$ and through a comparison with the pure phonon contribution of $LaPd_2Al_3$. Scattering of conduction electrons by phonons can be considered nearly independent of Ni doping or pressure, becoming irrelevant at low temperatures. Examples of fits obtained by applying (equation (2)) to experimental data are included in figure 5, whereas in figure 9 we have collected all θ_{tgh} values extracted by fitting $\rho_m(T)$ for different Ni concentrations and pressures (including $CePd_2Al_3$ [16] up to 64 kbar).

The $\theta_{tgh}(p, x)$ dependence, depicted in figure 8, resembles the expression for the binding energy of a Kondo singlet $T_K \propto \exp(-1/|J_{ex}N_F|)$ [7]. Pressure and concentration dependences are scaled using coincidences in $\rho(T)$ extracted from figure 5. The relative change of θ_{tgh} with Ni concentration is $d \ln \theta_{tgh}/dx = 2.3$/Ni at. A similar comparison can be made with the pressure dependence, getting a ratio $d \ln \theta_{tgh}/dp = 0.042$ kbar^{-1}. Knowing from [10] the bulk modulus of $CePd_2Al_3$, $B_0 = 680$ kbar, one can evaluate an electronic Grüneisen parameter [28] as $\Omega_e = d \ln \theta_{tgh}/d \ln V = 28.5$. If the same calculation is done taking into account the volume change caused by alloying (see figure 1(a)) one obtains a 2.5 times larger value for Ω_e. This indicates that *chemical pressure* produces a stronger increase of θ_{tgh} than *hydrostatic pressure*, probably due to stronger modifications of the Fermi surface (including anisotropic effects) and the energy of the 4f level. In fact, figure 1(b) shows the opposite variation between Ce–TM and Ce–Al interatomic spacings by doping, whereas pressure effects are expected to reduce

interatomic spacings isotropically. In order to make a quantitative comparison between the fitting parameter $\theta_{tgh}(x)$ and the actual Kondo temperature, we have included in figure 8 the T_K^{GS} values extracted from the evolution of $\Delta S_m(T)$ (after [27]). We find that between $x = 0$ and 0.50, $\theta_{tgh}(x) \approx 2T_K^{GS}(x)$.

5. Summary

From a detailed investigation of the critical concentration region, we have confirmed that the AF order in $CePd_{2-x}Ni_xAl_3$ collapses at $x > 0.2$. Beyond that concentration remainder short range interactions, probably caused by geometrical frustration, are observed. Kitazawa *et al* [9] indicated that CeT_2Al_3 systems are likely to exhibit magnetic frustration, caused by the distorted-triangular-lattice alignment of the Ce ions in this $CaCu_5$-type structure. Therefore, the system at hand could be viewed as a unique one, where the role of magnetic frustration and its impact on the NFL behaviour can be studied.

Approaching the critical point a coexistence of two contributions to the specific heat is observed. The major one corresponds to a usual NFL contribution, whereas the minor one only appears in a restricted range of concentration around the QCP. The former dominates the low temperature entropy and is well accounted for by the function $C_{NFL}/T = \gamma_0(1 - \sqrt{T/T_0})$, predicted for a 3D-AF scenario of spin fluctuations [29]. The decrease of γ_0 between $x = 0.35$ and 0.50 can be related to the increase of T_K^{GS} in that range of concentration. Beyond the critical point the system keeps its NFL behaviour up to about $x = 1$, where the FL regime sets in. This indicates that the loss of magnetic order does not necessarily imply an immediate crossover to an FL behaviour. Because the first excited CEF level lies within the thermal range of our measurements, one can clearly distinguish between the GS hybridization ($\propto T_K^{GS}$) evaluated at low temperature and that observed at $T \geqslant 10$ K ($\propto T_K^{CF}$).

Doping and pressure effects were successfully compared by introducing a scaling parameter proportional to the Kondo temperature. This comparison corroborates that the effect of both control parameters is similar but not identical because chemical pressure produced by doping not only may affect the volume but also the chemical potential and the topology of the Fermi surface. Altogether, we have shown that a proper knowledge of the physical phenomena related to a critical point cannot be restricted to a peculiar aspect or to a narrow concentration region of the phase diagram. Since the effects of a QCP singularity also involve *pre*-and *post-critical* concentration regions besides a significant temperature range, it has to be investigated as a whole ensemble of related properties.

Acknowledgments

JGS and PP are Conicet fellows. This work was partially supported by the FWF-Conicet International Cooperation Program 097/02 and Austrian FWF P16370, P18054 and a Grant-in-Aid for Scientific Research from MEXT of Japan and the Romanian projects GAR-26/2005 and CEEX-RP-5/2005.

References

[1] See for example Senthil T, Sachdev S and Vojta M 2005 *Physica* B **359–361** 9
2006 *Proc. SCES'05* at press
[2] Steward G R 2001 *Rev. Mod. Phys.* **73** 797
[3] Vojta T 2000 *Ann. Phys., Lpz.* **9** 403
[4] Sereni J G 1998 *J. Phys. Soc. Japan* **67** 1767

Sereni J G 2000 *Physica* B **281/282** 337
[5] von Löneysen H 1999 *J. Magn. Magn. Mater.* **200** 532
[6] Pedrazzini P, Gomez Berisso M, Sereni J G, Caroca Canales N, Deppe M and Geibel C 2004 *Eur. Phys. J.* B **38** 445
[7] Doniach S 1977 *Physica* B **91** 231
[8] Sereni J G 2001 *J. Phys. Soc. Japan* **70** 2139
Sereni J G 2002 *Physica* B **320** 376
[9] Kitazawa H, Schank C, Thies S, Seidel B, Geibel C and Steglich F 1992 *J. Phys. Soc. Japan* **61** 1461
[10] Tang J, Matsushita A, Kitazawa H and Matsumoto T 1996 *Physica* B **217** 97
[11] Fujiwara K, Yamanashi Y and Kumagai K 1995 *Physica* B **206/207** 228
[12] Galatanu A, Hauser R, Hilsher G, Michor H, Naber L and Bauer E 2000 *Physica* B **281/282** 83
[13] Bauer E, Galatanu A, Rogl P, Gomez Berisso M, Pedrazzini P and Sereni J G 2002 *Physica* B **312/313** 464
[14] Isikawa Y, Sakai H, Mitzushima T, Kuwai T and Sakurai J 2002 *Physica* B **312/313** 259
[15] Drechler A and Eichler A 1996 *Z. Phys.* B **100** 343
[16] Hauser R, Bauer E, Galatanu A, Indiger A, Maikis M, Kirchmayr H, Ginoux D and Schmitt D 1995 *Physica* B **206/207** 231
[17] Hausen M and Anderko K (ed) 1958 The atomic radius corresponds to the Goldschmit radius *Constitution of Binary Alloys* (New York: McGraw-Hill) Table B
For Ce, the radius corresponds to the Ce^{3+} configuration: Sereni J G 1982 *J. Less Common Met.* **84** 1
[18] Gopal E S R 1966 *Specific Heat at Low Temperatures* (London: Keywood Books)
[19] Krishna-Murthy H R, Wilson K G and Wilkins J W 1975 *Phys. Rev. Lett.* **35** 1101
[20] Hewson A 1993 *The Kondo Problem to Heavy Fermions* (Cambridge: Cambridge University Press)
[21] Schlottmann P 1983 *Z. Phys.* B **51** 223
[22] Moriya T and Takimato T 1995 *J. Phys. Soc. Japan* **64** 960
[23] Bruno E, Ginatempo B, Giuliano E S, Ruban A V and Vekilow Yu Kh 1994 *Phys. Rep.* **249** 354 and references therein
[24] Aoki Y, Urakawa J, Sagawara H, Sato H, Fukuhara T and Maezawa K 1997 *J. Phys. Soc. Japan* **66** 2993
[25] Dönni A, Furrer A, Kitasawa H and Zolliker M 1997 *J. Phys.: Condens. Matter* **9** 5921
[26] Desgranges H-U and Rasul J W 1985 *Phys. Rev.* B **32** 6100
[27] Desgranges H-U and Schotte K D 1982 *Phys. Lett.* A **91** 240
[28] Thompson J D and Lawrence J M 1994 *Handbook for Physics and Chemistry of Rare Earths* vol 19, ed K A Gschneidner Jr and L Eyring (Amsterdam: Elsevier Science) chapter 133
[29] Ioffe L B and Millis A J 1995 *Phys. Rev.* B **51** 16151